

The J Integral Evaluation of a Nozzle Corner Crack Under Thermal Transient Loading Condition

H. Miyamoto, M. Kikuchi

Department of Mechanical Engineering, Science University of Tokyo, 2641 Higashi Kameyama, Noda, Chiba 278, Japan

T. Okazaki, M. Kubo

Kure Works, Babcock Hitachi K.K., 6-9, Takara-machi, Kure-shi, Hiroshima 737, Japan

Summary.

This paper presents the results of the evaluation of the three dimensional J integral of a nozzle corner crack which is initiated by fatigue under thermal transient loading conditions of a BWR type reactor vessel. Analyses are carried out by using the finite element method in the following two cases. One case considers the effect of the stainless steel cladding deposited over the inside surface of the reactor vessel, and the other neglects it. In both cases, the extended J integral concept, called \hat{J} integral, is used to obtain the path independent J value in the thermal stress fields.

For the former case, considering the cladding, the \hat{J} integral is again extended to the crack problem in the multi-phase material, because the material properties are different between two materials, and the path independency of the \hat{J} integral no longer holds in such materials. The extension is carried out by introducing a new line integral term corresponding to the phase boundary.

By changing the shapes and the dimensions of the crack, some elastic analyses are carried out in the two dimensional space. The effects of the cladding are studied qualitatively, and the \hat{J} integrals are compared with the critical J value, and discussed.

Three dimensional J values along the three dimensional crack front are evaluated for the embedded crack. The results are compared with those for two dimensional analysis.

The nozzle corner crack is treated under thermal transient condition and distributions of \hat{J} value, and their change with time are obtained. The shapes and dimensions are changed by the assumption that the crack growth occurs at the point where the \hat{J} vector is the maximum, and the three dimensional shape of the propagating crack is estimated.

1. Introduction.

In the pressure vessel of the reactor, many kinds of thermal stress cycles exist, i.e. the stop and start of the reactor, and the circulation of the coolant, which may be related to thermal fatigue and it is pointed out that the probability of crack initiation and propagation exists. In United States, recently many papers have been published on the crack propagation and arrest problems under thermal shock accidents [1,2]. In these studies, K value of a crack is estimated and is compared with the K_{IC} and K_{IA} value, and the integrity of the vessel is discussed.

The reactor vessel is made of A533B steel, high toughness material, so it is desirable to evaluate the parameter of fracture in the elasto-plastic states, that is, the J integral is available as well as the K value. The J integral concept has been extended to the thermal stress field problem, by Aoki et al. [3], which is called \hat{J} integral.

On the other hand, as pointed out by Kryter et al. [4], the effects of the cladding, deposited on the inner surfaces of many reactors, have not yet been thoroughly studied. This is because of the complexity of the problem. That is, by the deposition of the cladding, there exists residual stresses, and differences of the material constants from the base material. So in this paper, a new concept of the \hat{J} integral, extended for the multi-phase material, is used to evaluate the \hat{J} value of a crack in the multi-phase material under thermal transient condition.

In the following, at first, two dimensional analyses are carried out for both cases, with and without cladding. The effects of the cladding on the changes of the \hat{J} value are shown and by comparing with the toughness value, the potential for fracturing is discussed. Then the three dimensional embedded crack at the phase boundary between base metal and cladding is treated. In this case, the \hat{J} vector is evaluated along the curved crack front from the three dimensional characteristics of the problem. Finally, the nozzle corner crack is analyzed both under inner pressure and thermal transient conditions. The shape and the dimension of the crack are changed and the shape of the propagating crack is estimated.

2. J integral in the thermal stress field and its extension to the multi-phase material.

Consider a two dimensional crack in an elastic body subjected to thermal stress as shown in fig.1. O-X1-X2 is the fixed frame and Γ denotes an arbitrary contour surrounding the crack tip O. A is an area surrounded by the contour Γ and the crack surfaces. The generalized force acting on the crack tip is represented by the \hat{J} integral as follows:

$$\hat{J}_\ell = \int_\Gamma (W^e \delta_{j\ell} - \sigma_{ij} u_{i,\ell}) ds_j + \int_A \sigma_{ij} \varepsilon_{ij,\ell}^* dA \quad (1)$$

where W^e is elastic strain energy density, u_i denotes displacement, σ_{ij} is stress tensor and ε_{ij}^* is thermal strain tensor.

The \hat{J} integral modified for the multi-phase material is expressed by:

$$\hat{J}_\ell = \int_{\Gamma_1-\Gamma_2} (W^e \delta_{j\ell} - \sigma_{ij} u_{i,\ell}) ds_j + \int_{A_1-A_2} \sigma_{ij} \varepsilon_{ij,\ell}^* dA \quad (2)$$

where Γ_1 , Γ_2 , A_1 , and A_2 are shown in Fig.2 5 .

The physical meaning of the modified \hat{J} integral is the generalized force acting at a crack tip, that is, terms concerning Γ_1 and A_1 give the generalized force acting on both a crack tip and singularities on the phase boundary, and terms concerning Γ_2 and A_2 give the force only on the latter. By subtracting the latter from the former, the generalized force acting at a crack tip can be evaluated.

3. Two dimensional analysis on the effect of cladding.

The effect of vessel cladding is analyzed by using the modified \hat{J} integral in multi-phase material. The path independency of the modified \hat{J} integral is shown in Fig.3.

An embedded crack and its model for analysis are shown in Fig.4. The model is simplified corresponding to cracks in cladding and in base metal, respectively.

The material properties used in the analysis are shown in Table I. Thermal and pressure loadings are: (a) inner pressure is zero, (b) initial wall temperature is 573 K, and (c) coolant temperature is 294 K. Heat transfer coefficients of the cladding and the base metal are assumed to be same. The residual stresses due to cladding are neglected here.

Fig.5 shows the \hat{J} integral when the crack tip is in the cladding for both cases, with and without cladding. The \hat{J} integral with cladding is greater than that without cladding, which is nearly half of the former. As the crack length becomes large, the differences between both values becomes small.

Fig.6 shows the \hat{J} value when the crack exists in the base metal and the crack tip coincides with the phase boundary. In this case, the \hat{J} values for both cases are nearly same.

The potential of the crack propagation can be discussed by comparing those \hat{J} values with the critical J_{IC} values of each material. In the RPV problem, the embrittlement by irradiation must be considered when the toughness of the material is discussed. Irradiation data for A533B steel is now being compiled, but that for stainless steel is scarce, so in this paper, we discuss the safety of the vessel by using the typical J_{IC} values at room temperature. For A533B steel, J_{IC} is nearly 245 kN/m, and for stainless steel, J_{IC} is considered to be 393 kN/m, which is nearly two-times larger than that of base metal.

In comparing these values with the \hat{J} values, it is noticed that when the crack tip is in the cladding, Model 4(a), the \hat{J} value and J_{IC} both are nearly twice those without cladding. So it is estimated that the potential of the fracture of the vessel is nearly same for both cases. In the Model

4(b), the \hat{J} values are the same but the toughness is twice that for the case with cladding, and it is concluded in this case that the condition with the cladding is safer than that without cladding.

4. Three dimensional analysis on the effect of cladding.

A three dimensional model of an embedded crack, shown in Fig.7, is analyzed. The shape of the crack is semi-circular and it exists in the base metal. Along the crack front, \hat{J}_x and \hat{J}_y , which are components of the \hat{J} vector are evaluated.

Fig.8 shows the \hat{J}_x and \hat{J}_y distributions along the curved crack front B-C. \hat{J}_x value becomes small as θ increases, but \hat{J}_y becomes large and then small as θ increases. This is because the crack closes at point C. Fig.9 shows the distributions of \hat{J} vector around the crack front. It is noticed that the maximum point of the \hat{J} value is at the phase boundary of the cladding, and it agrees well with that for two dimensions.

Fig.10 shows the comparison of \hat{J} values of points A and B in Fig.10, with two dimensional analyses. It is noticed that the two and three dimensional analyses agree very well quantitatively, so it is enough to discuss the effect of the cladding only by two dimensional analyses.

5. J vectors of nozzle corner crack of pressure vessel.

Fig.11 shows the shape and dimensions of the nozzle corner of the pressure vessel and a crack initiated at the corner. The boundary conditions are: (a) the initial temperature is 573 K, (b) the coolant poured from the nozzle is 373 K, and the coolant temperature is assumed to change gradually.

Three kinds of shapes of the nozzle corner crack are considered, as shown in Fig.12 (a), (b), and (c). At first, Model (a) is analyzed. The \hat{J}_x and \hat{J}_y components are shown in Fig.13(a) and (b) for different time steps. Both value becomes larger with the lapse of time. \hat{J} values reach the maximum at the nozzle surface and become smaller along the crack front. But the \hat{J}_y components are not the maximum at the vessel wall. They become larger near the nozzle surface, and again become small at the vessel wall. But the \hat{J}_y value near the vessel wall increases gradually with time lapse. This is because the gradient of the temperature increases along the vessel wall. In Fig.14 the magnitude of the \hat{J} vector is shown. It is noticed that for every time step, the \hat{J} value reaches the maximum at the inner surface of the nozzle, not at the vessel wall. The direction of the \hat{J} vector is nearly perpendicular to the crack front in every case. By assuming that the crack growth occurs where the \hat{J} value is the maximum, the new crack is modelled as shown in Fig.12(b). Then the model (b) is analyzed for the same boundary conditions. The same procedure is carried out and the model (c) is analyzed. Fig.15 and 16 show the \hat{J} vector distribution for 2 models. In every case, \hat{J} value is the maximum at the nozzle wall.

Fig.17 shows the results when the vessel is subjected to an inner pressure, p of 0.7 kgf/mm. In this case, J values at the vessel wall ($\theta=90^\circ$

) and at the nozzle wall ($\theta=0^\circ$) are nearly the same. Because of the properties of elasticity, superimposing is possible. Fig.18 is the results of superimposing the results of thermal loading on those of inner pressure. In this case, though the conditions of the inner pressure contribute largely to the J value, it becomes the maximum at the nozzle wall.

Now it is concluded that if the crack is propagated by fatigue, that is, with little plastic deformation, the results obtained above are applicable and the crack may be propagated along the nozzle surface.

Summary

- (1) The effects of cladding are analyzed by using the modified \hat{J} integral and it is shown that the cladding acts as a barrier to the embedded crack.
- (2) Three dimensional analysis is carried out on the cladding problem, and compared with two dimensional. Both agree quantitatively, so it is shown that two dimensional analyses are adequate for discussion of the effects of cladding.
- (3) The \hat{J} vectors of the nozzle corner crack are evaluated under both thermal and inner pressure conditions. \hat{J} values near the nozzle surface are always the maximum and it is estimated that the fatigue crack may be propagated along the nozzle surface.

REFERENCES

- [1] Cheverton, R.D., et al., NREG/CR-0107, ORNL/NUREG-40, (1981)
- [2] Iskander, S.K., et al., NUREG/CR-2113, ORNL/NUREG-84, (1980)
- [3] Aoki, S., et al., J. of Applied Mechanics, vol.48, (1981), pp.825
- [4] Kryter, R.C., et al., NUREG/CR-2083, ORNL/TM-8072, (1981)
- [5] Miyamoto, H., and Kikuchi, M., Numerical Methods in F.M., Eds. Owen, D.R.J., and Luxmoore, A.R., (1980), pp.359

Table I. Material properties for the analysis.

	base metal	clad
Young's modulus (GPa)	205.94	195.94
Poisson's ratio	0.3	0.3
Coefficient of thermal expansion (1/°K)	4.027×10^{-8}	5.858×10^{-8}
Thermal conductivity (W/m°K)	41.53	16.85
Thermal diffusivity (m ² /s)	1.056×10^{-5}	4.139×10^{-6}
Heat transfer coefficient (W/m ²)	1.136×10^3	1.136×10^3

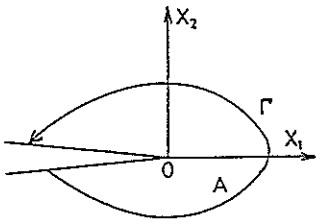


Fig. 1. Crack and the contour for \hat{J} integral.

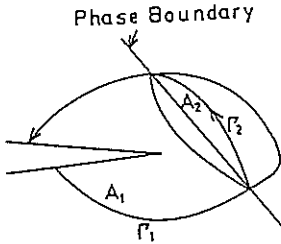
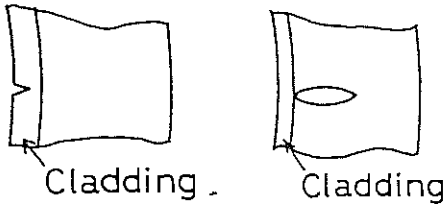


Fig. 2. Crack and the phase boundary.



(a) Crack is in the cladding. (b) Crack is in the base metal.

Fig. 4. Two dimensional model of cladding and a crack.

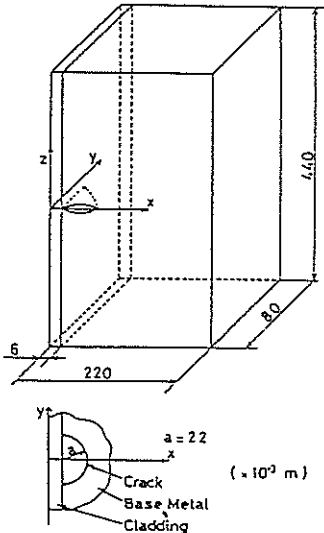


Fig. 7. Three dimensional model of cladding and a crack.

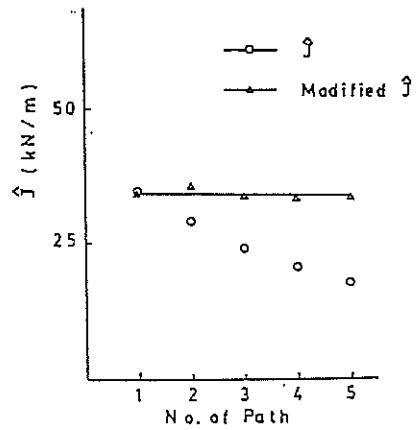


Fig. 3. \hat{J} value for each path.

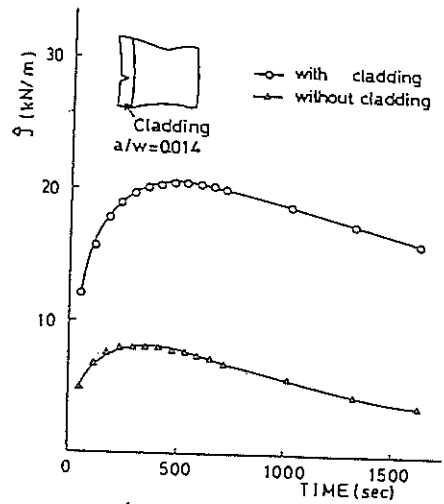


Fig. 5. \hat{J} value when the crack tip is in the cladding.

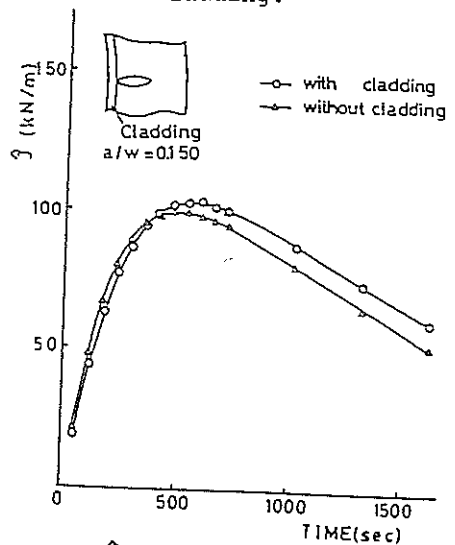
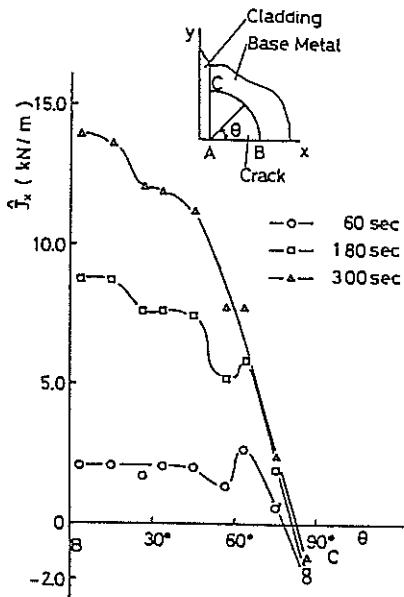
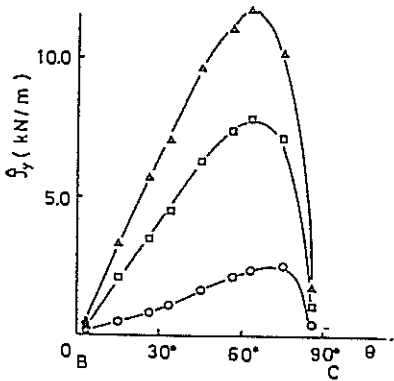


Fig. 6. \hat{J} value when the crack is in the base metal.



(a) \hat{J}_x value along the curved crack front.



(b) \hat{J}_y value along the curved crack front.

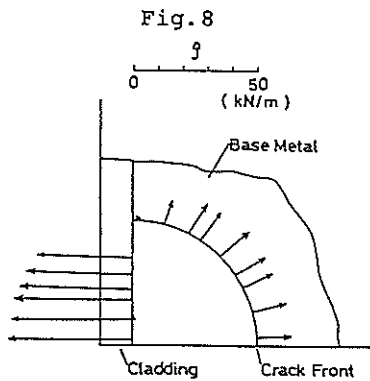


Fig.9 \hat{J} vector, distribution around the crack.

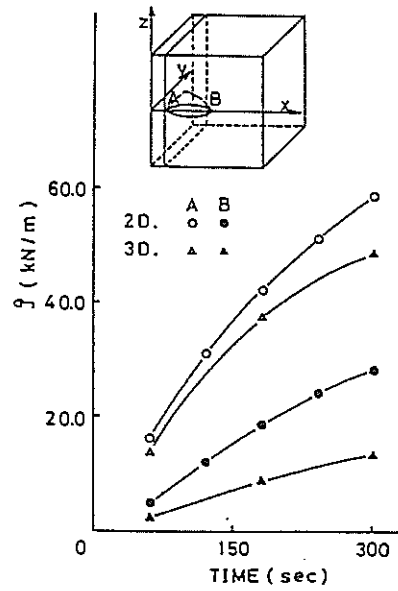


Fig.10 Comparison of 2d. and 3d. results.

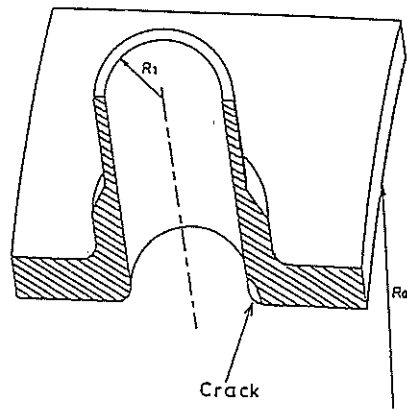
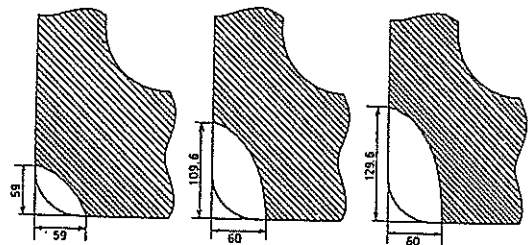
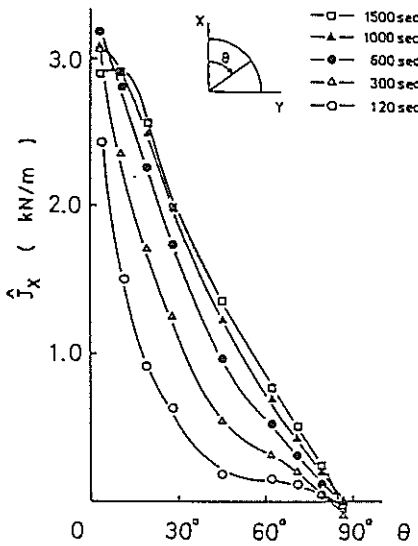


Fig.11 Model of a nozzle and a nozzle corner crack.

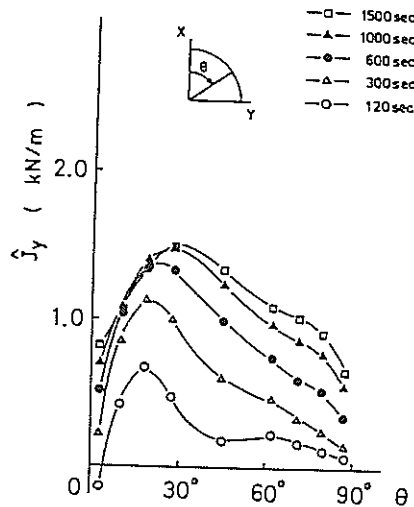


(a) case 1 (b) case 2 (c) case 3

Fig.12 Shapes of nozzle corner crack.



(a) \hat{J}_x for case 1.



(b) \hat{J}_y for case 1.

Fig.13

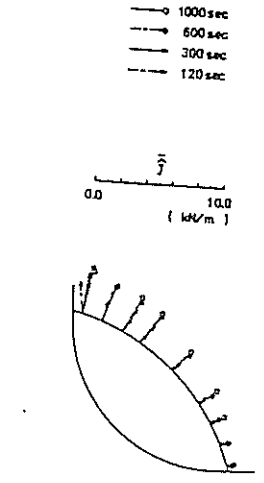


Fig.14 \hat{J} vector for case 1.

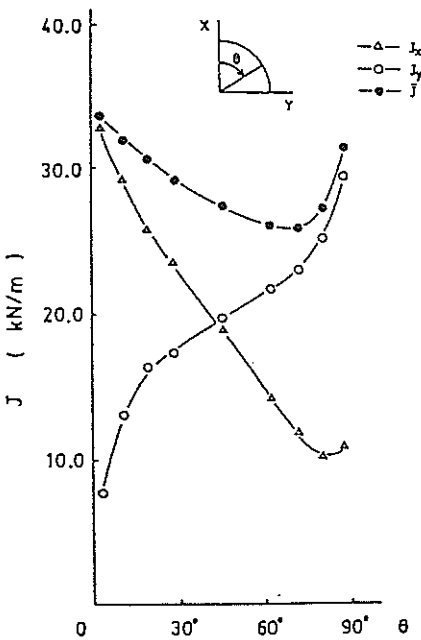


Fig.17 J vector for case 1 under inner pressure only.

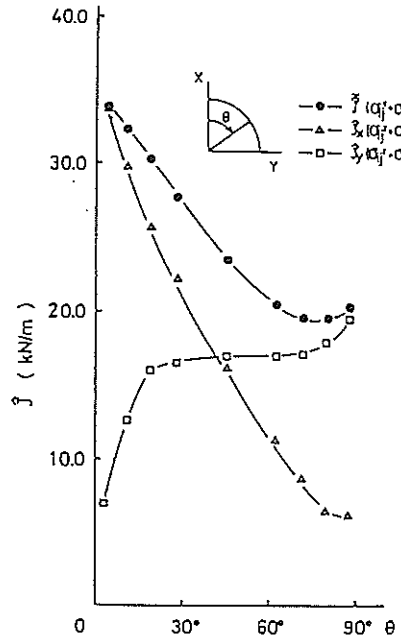


Fig.18 \hat{J} vector by thermal and pressure loadings.

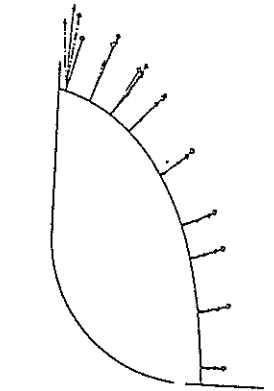


Fig.15 \hat{J} vector for case 2.

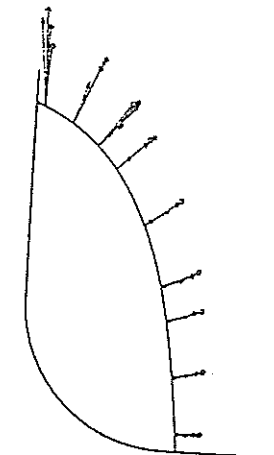


Fig.16 \hat{J} vector for case 3.